A Letters Journal Exploring the Frontiers of Physics

May 2010

EPL, **90** (2010) 44003
doi: 10.1209/0295-5075/90/44003

www.epljournal.org

Relaxation and flow in linearly sheared two-dimensional foams

M. E. Möbius[1,2(a)], G. Katgert[1] and M. van Hecke[1]

[1] *Kamerlingh Onnes Lab, Universiteit Leiden - Postbus 9504, 2300 RA Leiden, The Netherlands, EU*
[2] *School of Physics, Trinity College Dublin - Dublin 2, Ireland, EU*

received 20 October 2009; accepted in final form 5 May 2010
published online 7 June 2010

PACS 47.57.Bc – Complex fluids and colloidal systems: Foams and emulsions
PACS 83.60.Fg – Shear rate dependent viscosity
PACS 83.80.Iz – Emulsions and foams

Abstract – We probe the relation between rheology and shear-induced relaxation in experiments on two-dimensional foams at steady shear. The characteristic relaxation time t_r, which we extract from the non-affine part of the bubble displacements, scales non-linearly with the local strain rate $\dot{\gamma}$. In particular, the relative strength of the non-affine part grows when $\dot{\gamma} \to 0$ —hence the foam flow is *not* quasistatic down to the lowest experimentally accessible shear rate. Furthermore, we establish a direct connection between the relaxation time scaling and the macroscopic rheology.

Soft glassy materials, such as foams, emulsions, colloidal glasses and granular media, exhibit highly complex flows. On the local scale, rearrangements in these densely packed systems are erratic due to geometric frustration. Globally, the relation between strain rate $\dot{\gamma}$ and stress τ is generally non-linear, often taking a Herschel-Bulkley form: $\tau = \tau_Y + k\dot{\gamma}^\beta$, where τ_Y denotes the yield stress, and where the viscous stress $\tau_V \equiv \tau - \tau_Y$ scales non-linearly with the strain rate $\dot{\gamma}$ [1–3].

What is the connection between the macroscopic bulk rheology and the microscopic, dissipative rearrangements of these materials? For non-Brownian systems, such as foam, the strain rate controls the dynamics of these rearrangements. A fruitful strategy is therefore to characterize and compare the strain rate dependence of global stress and local relaxation events. For colloidal glasses, the microscopic relaxation times were found to scale non-linearly with the inverse local strain rate, but a direct and quantitative connection to the rheology has not been established, possibly because rearrangements are both shear induced and thermally activated in these systems [4–7].

Recent experiments and simulations on sheared foams have uncovered rich dynamics on the bubble scale [8–13]. However, the precise form of the dependence of relaxation time scales on the strain rate is not clear yet: while Diffusive Wave Spectroscopy measurements suggest a shear-induced rearrangement rate that is simply $1/\dot{\gamma}$ [8,9], rheological measurements [7,14] and simulations of the Durian bubble model [10] show a non-linear decrease in the relaxation time with shear rate. Moreover, a quantitative connection between the relaxation time scales and the bulk rheology of foams is lacking, except for ordered foams [15,16].

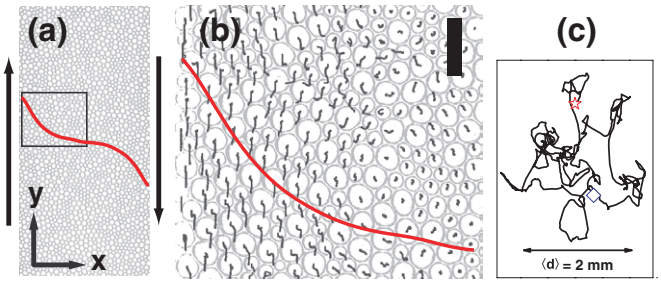

Fig. 1: (Color online) (a) Binarized image of the bubble layer viewed from the top with the region of interest highlighted by a box. The black arrows to the left and right indicate the applied shear velocity v_0 in opposite directions with equal magnitude. The red curve shows the velocity profile for $v_0 = 0.076\,\mathrm{mm/s}$. (b) Zoom of the highlighted region showing short time bubble trajectories. In this region, $\langle v_x(x)\rangle \approx 0$. The width of the black bar denotes the bin size $\Delta x = 1.6\,\mathrm{mm}$ used below. (c) Example of a non-affine bubble trajectory (*i.e.*, with average flow subtracted) over a period $\Delta t = 145\,\mathrm{s}$, for local strain rate $\dot{\gamma} = 0.03\,\mathrm{s}^{-1}$ at $v_0 = 0.62\,\mathrm{mm/s}$. The star and diamond symbol denote the start and endpoint, respectively, both of which are at $x = 3.5\langle d\rangle$.

In this letter we find a direct and quantitative relation between the strain rate dependencies of the microscopic relaxation time t_r and the macroscopic viscous stress τ_V

(a) E-mail: mobiusm@tcd.ie

in experiments on a sheared two-dimensional, disordered foam. We measure the relaxation dynamics directly by imaging and tracking the bubble motion in a linearly sheared foam. Our flow geometry, typical flow profiles and bubble trajectories are shown in fig. 1. Due to the presence of a top plate that covers the bubbles, the average flow profiles exhibit shear bands in our experiment [12,13,17–19] and we employ these to study the statistics of bubble displacements over a range of local strain rates $\dot{\gamma}$ spanning three decades. The rheology of this material is probed in rheometric measurements on freely floating 2D foams in a Couette cell [12,13,20].

First, we establish that the bubbles start to diffuse after a certain shear-rate–dependent relaxation time t_r, which is both reflected in the mean square displacements as well as the corresponding displacement PDFs. We use the Lindemann criterion to extract the relaxation time t_r as function of local strain rate $\dot{\gamma}$. We think of this time as the inverse rate of dissipative rearrangements.

Second, we find that t_r is not proportional to the inverse strain rate $1/\dot{\gamma}$, but instead exhibits non-linear scaling: $t_r \approx t_0^{1-\nu}\dot{\gamma}^{-\nu}$, where $\nu = 0.66 \pm 0.05$ and t_0 is a characteristic timescale, needed for dimensional reasons. This non-linear scaling implies that fluctuations become larger for smaller strain rates.

Third, we find that the non-linear scaling of the viscous stress with strain rate [12,19] can be directly related to the scaling of the relaxation time: $\tau_V \approx G_0\dot{\gamma}t_r$, where G_0 is the static shear modulus. This connection is consistent with a non-equilibrium Stokes-Einstein relation.

Our results link strain rate, relaxation time, and stresses. Our scenario is not particular to foams, and we suggest to probe similar connections in other sheared, non-Brownian systems, such as suspensions, granular media, emulsions and microscopic models of these.

Setup and tracking. – The measurements are performed in a linear shear cell (fig. 1) that is described in detail elsewhere [12,13]. We create a bidisperse foam layer with bubble diameters of 1.7 and 2.7 mm, respectively, that is floating on a surfactant solution (5% volume fraction Dawn dishwashing liquid, 15% glycerol and 80% demineralized water, viscosity $\eta = 1.8 \cdot 10^{-3}\,\mathrm{Pa \cdot s}$, surface tension $\sigma = 28 \cdot 10^{-3}\,\mathrm{N/m}$). The average bubble diameter $\langle d \rangle$ equals 2.0 ± 0.1 mm. The bubbles are trapped between the fluid layer and a glass plate placed 2.2 mm above the solution. The gap size between solution and top plate controls the packing fraction [13], which is 0.96 in the 2D projection of the bubble areas. Bubble coarsening is negligible over experimental time scales and we do not observe rupturing, coalescence or size separation of the bubbles. Local shear rates encountered in this experiment range from $3 \cdot 10^{-4}\,\mathrm{s}^{-1}$ to $0.3\,\mathrm{s}^{-1}$.

To induce shear, two rotating wheels of 39 cm diameter are partially immersed in the surfactant solution and spaced $7\,\mathrm{cm} = 35\langle d \rangle$ apart. The rotation speed of the wheels controls the driving velocity v_0 of the shearing boundary which we vary between 0.073 and 2.3 mm/s. For the subsequent measurements and analysis we focus on a region (fig. 1(a)) where the average flow transverse to the shear direction is absent: $\langle v_x(x) \rangle \approx 0$.

Tracking: We record the bubble motion by imaging the monolayer from above at 10 frames per second for 10^4 time steps. We illuminate the bubble layer from both sides, and view the bubbles from above. Even though the bubbles are in contact, as can be seen from the flattened contact lines, they appear as rings in our images (fig. 1(a), (b)). The bubbles change their shape during flow. We determine the initial bubble position, $\vec{r}_0$, from the center of mass of the bubble interior (area inside the rings). To track the bubbles through subsequent frames, we cross-correlate the bubble area with the bubble area in the next frame, and this allows us to determine the bubble displacements to about $0.005\langle d \rangle$ at each time step —bubble trajectories $\vec{r}$ are then reconstructed by adding subsequent displacements. We estimate the tracking error from the mean square displacement at zero applied shear —notice that the tracking error accumulates at each time step. As shown in fig. 2(b), the resulting virtual displacement due to tracking errors is well below the displacements at finite strain rate, and for the subsequent data analysis this tracking error is negligible. Our main experimental limitation is that for the lowest strain rates shown here, the data becomes increasingly noisy

Bubble diffusivity. – The local shear rate $\dot{\gamma} \equiv \partial v(x)/\partial x$ varies within the gap since the flows exhibit shear banding [12]. In order to relate the rearrangement rate of the bubbles to the local shear rate, we divide the measurement area into bins of size $\Delta x = 1.6 = 0.8\langle d \rangle$ mm (fig. 1(b)), for which we determine the local average flow $\langle \vec{v}(x) \rangle$ and shear rate $\dot{\gamma}$. We then measure the *non-affine* bubble tracks $\Delta\vec{s}(\Delta t)$ by subtracting the affine mean flow from the bubble trajectories $\vec{r}$: $\Delta\vec{s}(\Delta t) \equiv \vec{r}(t + \Delta t) - \vec{r}(t) - \langle \vec{v}(x) \rangle \Delta t$. An example of an erratic bubble trajectory $\Delta\vec{s}$ is shown in fig. 1(c). We only consider the mean square displacements on short time scales where $\langle \Delta s^2 \rangle \lesssim \langle d \rangle^2$, so that Taylor dispersion is negligible.

In fig. 2(a), the probability distribution functions (PDFs) of both the x and y component of $\Delta\vec{s}$ are shown for a given local shear rate $\dot{\gamma}$ at three different times as indicated. The widths of all distributions are normalized by $\sqrt{\langle \Delta s^2 \rangle}$ to highlight the qualitative changes in these PDFs with time. At all times, the fluctuations of the bubble trajectories are isotropic and the corresponding PDFs symmetric. On short time scales, the shape is non-Gaussian, similar to the instantaneous velocity fluctuations observed in a bubble raft[1] [11]. For longer time intervals, the PDFs develop exponential tails and eventually become Gaussian in the long time, diffusive

[1] The difference between our result and Wang's [11] regarding the symmetry of the PDFs is most likely due to the different degree of disorder. Wang's system is not bidisperse and contains more ordered domains.

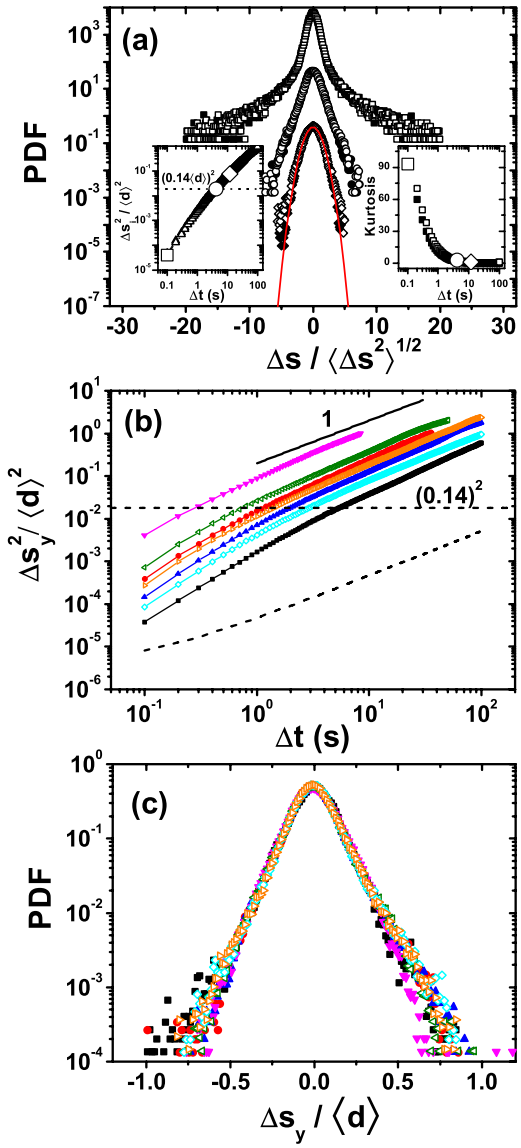

Fig. 2: (Color online) (a) Evolution of transverse (full symbols) and longitudinal (open symbols) non-affine displacement PDFs at $\dot{\gamma} = 0.005\,\mathrm{s}^{-1}$: $\Delta t = 0.1$ s (■, □); $\Delta t = 4.1$ s (●, ○); $\Delta t = 12.1$ s (♦, ◊). The PDFs are shifted for clarity and normalized by the width of the respective distributions. The red curve is a Gaussian distribution. Left inset: the corresponding longitudinal (△) and transverse (▲) mean square displacements as a function of time. Right inset: the Kurtosis $\langle \Delta s^4 \rangle / \langle \Delta s^2 \rangle^2 - 3$ for the transverse (full symbols) and longitudinal (open symbols) fluctuations. In both insets the three symbols denote the time for which the PDFs have been plotted. (b) Mean square displacements $\langle \Delta s_y^2 \rangle$ as a function of time at different local shear rates $\dot{\gamma}$ in units of s^{-1}: 0.002 (■); 0.009; (◊) 0.016 (▲); 0.028 (▷); 0.038 (●); 0.071 (◁); 0.29 (▼). The horizontal dashed line denotes the Lindemann criterion $\Delta s_y^2 / \langle d \rangle^2 = 0.14^2$. The black dashed curve provides a noise floor for our measurements, well below the curves at finite strain rate, and is obtained from the apparent mean square displacement at zero applied shear due to accumulation of tracking errors. (c) The PDFs of the mean square displacements at the Lindemann criterion exhibit exponential tails.

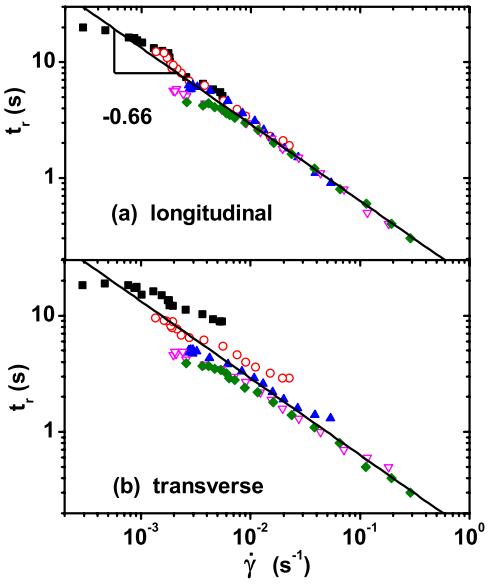

Fig. 3: (Color online) Longitudinal (a) and transverse (b) relaxation time as a function of local shear rate for different driving velocities: $v_0 = 0.076$ mm/s (■); $v_0 = 0.25$ mm/s (○); $v_0 = 0.62$ mm/s (▼); $v_0 = 1.5$ mm/s (▽); $v_0 = 2.3$ mm/s (♦). t_r is defined as $\langle \Delta s_y^2 \rangle (\Delta t = t_r) = (0.14\langle d \rangle)^2$. The line is a fit to the data in (a): $t_r = t_0^{0.34} \dot{\gamma}^{-0.66}$.

regime. This behavior is also reflected in the evolution of the Kurtosis (right inset of fig. 2(a)). This behavior should be compared to sheared glasses, where the PDFs were found to have exponential tails for a range of early times before crossing over to Gaussian behavior at late times [21–23].

In fig. 2(b) we show the longitudinal mean square displacements for a range of local shear rates as a function of time. We have checked that our results only depend on the local shear rate by varying both the driving velocity v_0 and location of the bin. We notice that the characteristic time for crossover from super-diffusive to diffusive behavior is of the same order of magnitude as the time where the mean square displacement is $\Delta s_y^2 (t = t_r) = (0.14\langle d \rangle)^2$ which corresponds to the Lindemann criterion for melting in atomic solids and cage breaking in colloidal suspensions [4]. We use the Lindemann criterion to determine a relaxation time, t_r, and note that at this time the tails of the PDFs become exponential (fig. 2(c)). Hence, this empirical definition captures an important timescale in our system.

Relaxation time. – We now extract t_r for a range of local shear rates $\dot{\gamma}$ at different driving velocities v_0 for both the longitudinal and transverse fluctuations (fig. 3). Since Brownian fluctuations do not play a role, the rearrangements in the foam are entirely shear induced, and *a priori* $\dot{\gamma}^{-1}$ would be a prime candidate for setting the relaxation time. In contrast, we find that $t_r = t_0^{1-\nu} \dot{\gamma}^{-\nu}$, where $\nu \approx 0.66 \pm 0.05$, and t_0 is a timescale, that has a value of $2.9 \times t_{char}$, where t_{char} is the characteristic

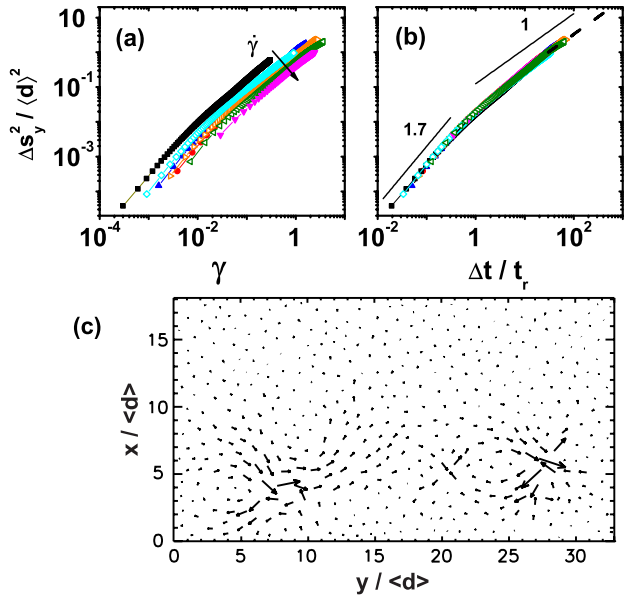

Fig. 4: (Color online) (a-b) The non-affine mean square displacement $\langle \Delta s_y^2 \rangle$ for different local shear rates (same data as in fig. 2(b)) *vs.* local strain $\gamma = \dot{\gamma}\Delta t$ (a) and *vs.* dimensionless time $\Delta t / t_r(\dot{\gamma})$ (b). The dotted line in (b) indicates the diffusive limit. (c) Typical snapshot of $\Delta \vec{s}$ for $v_0 = 0.62\,\mathrm{mm/s}$, $\Delta t = 0.1\,\mathrm{s}$. Localized events involving large displacements are clearly visible.

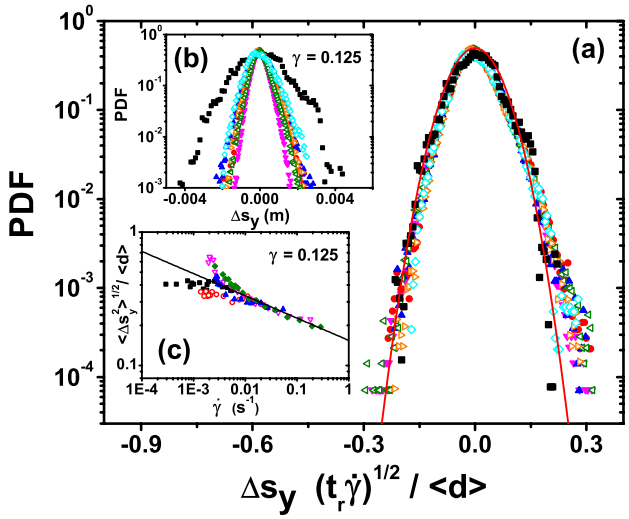

Fig. 5: (Color online) The PDFs of the non-affine longitudinal displacement Δs_y at *fixed local* strain $\gamma = 0.125$ for different local strain rates —the data is the same as used in fig. 2(b). Main panel: PDFs plotted for the rescaled displacements $\sqrt{\dot{\gamma} t_r}(\Delta s_y / d)$. The red curve is a Gaussian fit to the data. Top inset: PDFs for the unscaled displacements Δs_y. Bottom inset: The scaled root mean squared displacement $\sqrt{\langle (\Delta s_y/d)^2 \rangle}$ at $\gamma = 0.125$ *vs.* local strain rate for different driving velocities: $v_0 = 0.076\,\mathrm{mm/s}$ (■); $v_0 = 0.25\,\mathrm{mm/s}$ (○); $v_0 = 0.62\,\mathrm{mm/s}$ (▲); $v_0 = 1.5\,\mathrm{mm/s}$ (△); $v_0 = 2.3\,\mathrm{mm/s}$ (♦). The line denotes a power law fit with exponent $-1/6 \approx (\nu - 1)/2$.

relaxation time of single bubbles $\eta \langle d \rangle / \sigma = 1.3 \cdot 10^{-4}\mathrm{s}$ [24] —see fig. 3. This scaling is our first central result. Note that although the scaling collapse for the transversal fluctuations is less satisfying than for the longitudinal fluctuations at low shear rates, the overall result is similar.

We now use our findings to collapse the mean squared displacement curves onto a single master curve. Figure 4(a) illustrates that the system is not quasi-static[2], in the sense that the non-affine mean square displacements do not simply scale with strain. In fact, fig. 4(a) shows that for a given local average strain, Δs_y^2 is larger in regions where the local shear rate is smaller —*fluctuations thus increase for slower flows*. Figure 4(b) shows that it is possible to obtain good data collapse by rescaling the time axis with the relaxation time.

Figures 4(a), (b) illustrate that for early times we observe super-diffusive behavior with initial slope ≈ 1.7 for short times — we do not see a ballistic regime. We believe this is due the large and localized non-affine displacements observed even on the shortest time scales (fig. 4(c)). Moreover, these events may also be responsible for the fat tails in the non-affine displacement PDFs shown in fig. 2(a).

[2]It may seem counter-intuitive that our system is not quasistatic, given that the single bubble relaxation time t_{char} [24] is several orders of magnitude smaller than the typical inverse shear rate in our system. However, since the fluid flow is concentrated in the thin liquid films separating the bubbles ($h \approx 10^{-7}$–10^{-6} m [15]), the effective shear rate $\dot{\gamma}_{eff} = \langle d \rangle \dot{\gamma} / h$ in these films is much closer to $1/t_{char}$.

At later times the bubbles become diffusive and the slope approaches 1. From the collapse shown in fig. 4(b) we deduce that the diffusion constant D_y scales non-linearly with the shear rate $\dot{\gamma}$ as $D_y = (0.017 \pm 0.002)\langle d \rangle^2 / t_r$. Similar results are found for the transverse fluctuations. By combining the scaling of the diffusion constant with the definition $\Delta t = \gamma\, \dot{\gamma}^{-1}$, we find that $\langle (\Delta s_y/d)^2 \rangle \propto \Delta t / t_r \propto \gamma\, \dot{\gamma}^{\nu-1}\, t_0^{\nu-1}$. Hence, the mean squared displacements in the diffusive regime, measured at a fixed, sufficiently large strain γ, grow as $\dot{\gamma}^{\nu-1}$ when $\dot{\gamma}$ is lowered.

Figure 5 illustrates that not only the second moment $\langle (\Delta s_y/d)^2 \rangle$, but the entire PDF of the non-affine displacements obey this scaling relation: the PDFs of $(\Delta s_y/d)\sqrt{t_r/\Delta t}$ exhibit scaling collapse, while similar to the absence of data collapse shown in fig. 4(a), the PDFs for the unscaled Δs do not collapse. Finally, the root mean squared displacements taken over the entire gap and for different driving velocities but at fixed strain $\gamma = 0.125$ indeed scale as $\sqrt{\Delta t / t_r} \sim \dot{\gamma}^{(\nu-1)/2}$ (lower inset of fig. 5).

Rheology. – We will now establish a surprising relation between relaxation times and rheology. For the rheology measurements we employ a Couette cell *without* a top plate in order to measure the stress-strain rate relation of the 2D foam directly [12,13]. The inner and outer radius are $r_i = 5\,\mathrm{cm}$ and $r_o = 7\,\mathrm{cm}$, respectively, and the gap has grooves on both sides to prevent slip of the bubbles. The inner wheel is connected to a MCR 301 rheometer head

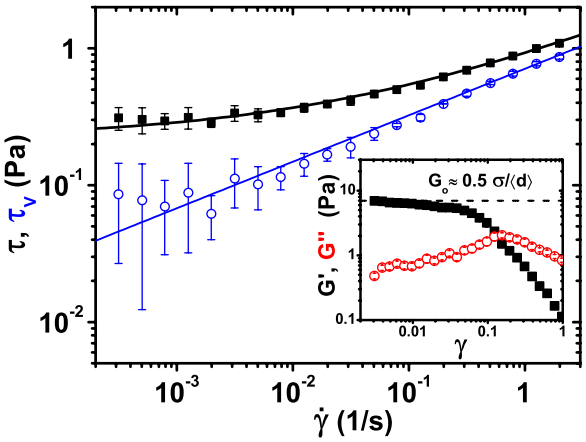

Fig. 6: (Color online) Foam rheology. The stress is plotted as a function of shear rate measured in a Couette cell with inner radius 5 cm and outer radius 7 cm. The disordered foam is floating on the soap solution without the top plate and the boundaries have grooves to prevent bubble slip. The shear rate at the inner rotating wheel has been determined by image velocimetry. ■: total stress. The Herschel-Bulkley exponent is $\beta = 0.36 \pm 0.05$. The black curve through the data is $G_0\,(\gamma_Y + 0.83\ t_r\dot{\gamma})$; ○: viscous stress $\tau_V \equiv \tau - \tau_Y$, where $\tau_Y = 0.22 \pm 0.2$ Pa. The blue curve through the data is $0.83\ t_r\dot{\gamma}$. Inset: Oscillatory strain sweep at 0.1 Hz. G' approaches the static shear modulus G_0 at low strain amplitude: $G_0 \approx 7$ Pa and the static yield strain $\gamma_Y = 0.031$.

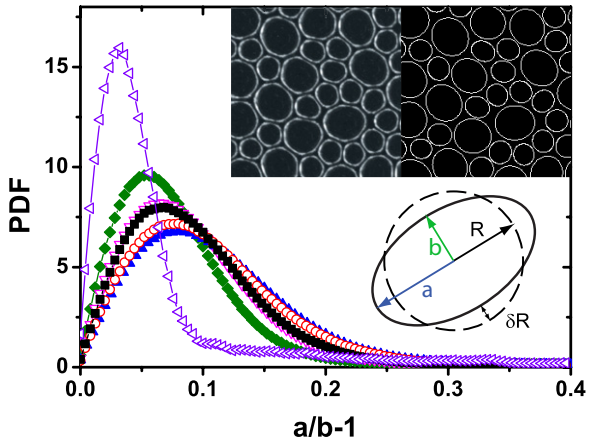

Fig. 7: (Color online) Bubble deformations measured by a/b, the ratio of the semimajor and semiminor axes of elliptical fits to the deformed bubbles. Main panel: the PDFs of $a/b - 1$ for all the bubbles do not exhibit a trend with the driving velocity v_0: 0.076 mm/s (■); 0.25 mm/s (○); 0.62 mm/s (▲); 1.5 mm/s (△); $v_0 = 2.3$ mm/s (♦). The peak positions of the PDFs of the flowing system differ significantly from the static case (◁). Inset: Snapshot of part of the system (left image) and the corresponding elliptical fits (right image). Sketch in the right bottom corner indicates the bubble deformation δR.

from Anton Paar that has a 0.1 μNm torque resolution in this setup, which corresponds to a stress resolution of $d\tau = 0.1\,\mu\text{Nm}/(2\pi r_i^2 \cdot \langle d\rangle) = 3$ mPa. In order to minimize the drag with the fluid, the inner wheel is made hollow, so that only the outer rim (≈2 mm thick) of the inner wheel is in contact with the surfactant solution underneath. The residual inner wheel drag with the underlying fluid has been accounted for by measuring the torque without the bubbles present, and is subtracted from all the foam rheology measurements. It is also important to note that at high rotation rates the drag of the bubbles with the underlying fluid becomes appreciable. We measured this drag by shearing a bubble layer that is not in contact with the outer ring of the Couette cell so that bubble layer moves as a solid body. Since this drag cannot easily be compensated, we probed the rheology up to $\dot{\gamma} = 2\,\text{s}^{-1}$ where the bubble-fluid drag is less than 10% of the raw stress.

Figure 6 illustrates that our 2D foams exhibits a Herschel-Bulkley type rheology, with the shear stress τ equal to the sum of a yield stress τ_Y and the rate-dependent viscous stress $\tau_V = k\dot{\gamma}^\beta$ [12]. Our second central result is that the plastic viscosity $\eta_p \equiv \tau_V/\dot{\gamma}$, is just proportional to the relaxation time t_r. This provides a connection between the macroscopic rheological exponent β and the microscopic relaxation time exponent ν: within experimental error $\beta \approx 1 - \nu$ (see footnote [3]).

[3]The top plate introduces a body force, but does not affect the foam rheology [12,13] —we tacitly assume that the relaxation times are unaffected as well.

This connection between the viscous stress τ_V and t_r can be made intuitive by defining a characteristic strain $\gamma_c = t_r\dot{\gamma}$. The characteristic strain is thus increasing with shear rate, which is consistent with observations by Rouyer *et al.* [25]. To convert this characteristic strain into a stress, we multiply it with the static shear modulus G_0 which we measured to be $\mathcal{O}(\sigma/\langle d\rangle)$ (see inset of fig. 6) consistent with Princen *et al.* [26]. As fig. 6 shows, $G_0\gamma_c$ and the viscous stress τ_V are equal up to a numerical factor of order one: $\tau_V = 0.83\ G_0 t_r\dot{\gamma}$. Hence the non-linear global rheology of our foams, and in particular the non-linear scaling of the plastic viscosity, is connected to a shear-rate–dependent relaxation time t_r on the bubble scale.

Stokes-Einstein relation. – In previous numerical work on sheared foams, a non-equilibrium Stokes-Einstein relation was found to relate the product of diffusion constant, viscosity and bubble size to an energy scale obtained from fluctuations in the elastic energy [10,27]. We show now that our connection between relaxation time and viscous stress may also be viewed from this perspective.

Both the diffusion constant $D_y \propto \langle d\rangle^2/t_r$ and the plastic viscosity $\eta_p \propto G_0 t_r$ are shear rate dependent, but this dependence drops out in the product of these two quantities. Hence, multiplying the plastic viscosity with the diffusion constant and average bubble size, we obtain an energy scale that is constant in the experimentally accessible range of shear rates: $E = D_y\eta_p\langle d\rangle \approx 7 \cdot 10^{-3}\,\sigma\langle d\rangle^2$. The rate independence of this energy scale is consistent with simulation results at low shear rates [27].

How does this energy scale compare to elastic energy fluctuations of the bubbles? The elastic response of a single bubble can be modeled by a spring with spring constant

$4\pi\sigma$ [28], so that the energy of a single deformation δR equals $2\pi\sigma\delta R^2$. In fig. 7 we estimate the elastic energy fluctuations by fitting an ellipse to the deformed bubbles and extract the semimajor (a) and semiminor (b) axes of the ellipse. Assuming that the bubble typically experiences two stronger and opposite contacts and preserves volume, then $a = R + \delta R$ and $b = R - \delta R$, so that $a/b - 1 \approx 2\delta R/R$. The deformations captured by $a/b - 1$ do not show a trend with driving rate. The corresponding energy fluctuations of the two contacts can be obtained by computing $2\langle\delta E\rangle \equiv 2\sqrt{\langle E^2\rangle - \langle E\rangle^2} = 4\pi\sigma\sqrt{\langle\delta R^4\rangle - \langle\delta R^2\rangle^2}$. We infer the moments of δR from the PDFs of the flowing foam in fig. 7. For all the PDFs, $\langle\delta R^4\rangle \approx 3\cdot 10^{-5}R^4$ and $\langle\delta R^2\rangle \approx 3\cdot 10^{-3}R^2$. After substituting we find that $2\langle\delta E\rangle \approx 0.01\sigma\langle d\rangle^2$, which is of similar magnitude as the elastic energy fluctuations obtained previously from the Stokes-Einstein relation.

Discussion. – Our first central result is the scaling of the relaxation time with shear rate: $t_r \approx t_0^{1-\nu}\dot{\gamma}^{-\nu}$. Defining quasistatic flows as those for which statistical properties of the bubble trajectories depend only on strain, the nonlinear scaling of t_r and figs. 4 and 5 clearly show that our flows are inconsistent with such a quasistatic picture, even though the global stresses approach rate independence for slow flows. This so-called sub-linear scaling has been observed in simulations [10,29] (see footnote [2]).

Our second main result are the relations between relaxation time and rheology which we can rationalize by defining a characteristic strain, and which also can be understood via a Stokes-Einstein relation. Aspects of our scenario have been observed before in simulations: In thermal Lennard-Jones systems, for example, a qualitative relation between viscosity and relaxation time has been found [5], while simulations of athermal sheared systems (models for foams) established a Stokes-Einstein relation connecting diffusivity, viscosity and stress fluctuations [10,27].

We hope that our work stimulates further studies in which the simple connections between all main ingredients, *i.e.*, relaxation time, non-affine fluctuations, rheology and (elastic) stress fluctuations are probed in a wider range of systems. The microscopic scenario which emerges is that for increasingly slow flows, the delicate balance between elastic and viscous forces [30] causes the (relative) bubble motion to become increasingly erratic. What remains a puzzle is to understand how these slow flows combine rate independence of the average stresses and the elastic energy fluctuations with increasingly large microscopic fluctuations and a growing relaxation time.

* * *

The authors wish to thank J. Mesman for technical assistance, and discussions with R. Besseling, T. Witten and W. van Saarloos are gratefully acknowledged. GK and MEM acknowledge support from physics foundation FOM.

REFERENCES

[1] Larson R. G., *The Structure and Rheology of Complex Fluids* (Oxford University Press, New York) 1999.
[2] Höhler R. and Cohen Addad S., *J. Phys.: Condens. Matter*, **17** (2005) R1041.
[3] Weaire D. and Hutzler S., *The Physics of Foams* (Clarendon Press, Oxford) 1999.
[4] Besseling R., Weeks E. R., Schofield A. B. and Poon W. C. K., *Phys. Rev. Lett.*, **99** (2007) 028301.
[5] Varnik F. and Henrich O., *Phys. Rev. B*, **73** (2006) 174209.
[6] Schall P., Weitz D. A. and Spaepen F., *Science*, **318** (2007) 1895.
[7] Wyss H. *et al.*, *Phys. Rev. Lett.*, **2007** (98) 238303.
[8] Gopal A. D. and Durian D. J., *Phys. Rev. Lett.*, **75** (1995) 2610.
[9] Gopal A. D. and Durian D. J., *J. Colloid Interface Sci.*, **213** (1999) 169.
[10] Ono I. K., Tewari S., Langer S. A. and Liu A. J., *Phys. Rev. E*, **67** (2003) 061503.
[11] Wang Y., Krishan K. and Dennin M., *Phys. Rev. E*, **74** (2006) 041405.
[12] Katgert G., Möbius M. E. and van Hecke M., *Phys. Rev. Lett.*, **101** (2008) 058301.
[13] Katgert G., Latka A., Möbius M. E. and van Hecke M., *Phys. Rev. E.*, **79** (2009) 066318.
[14] Gopal A. D. and Durian D. J., *Phys. Rev. Lett.*, **91** (2003) 188303.
[15] Denkov N. D. *et al.*, *Phys. Rev. Lett.*, **100** (2008) 138301.
[16] Tcholakova S. *et al.*, *Phys. Rev. E*, **78** (2008) 011405.
[17] Janiaud E., Weaire D. and Hutzler S., *Phys. Rev. Lett.*, **97** (2006) 038302.
[18] Wang Y., Krishan K. and Dennin M., *Phys. Rev. E*, **72** (2006) 031401.
[19] Langlois V. J., Hutzler S. and Weaire D., *Phys. Rev. E*, **78** (2008) 021401.
[20] Denkov N. D. *et al.*, *Colloids Surf. A*, **263** (2005) 129.
[21] Tanguy A., Leonforte F. and Barrat J. L., *Eur. Phys. J. E*, **20** (2006) 355.
[22] Lemaître A. and Caroli C., *Phys. Rev. E*, **76** (2007) 036104; *Phys. Rev. Lett.*, **103** (2009) 065501.
[23] Chaudhuri P., Berthier L. and Kob W., *Phys. Rev. Lett.*, **99** (2007) 060604.
[24] Durian D., *Phys. Rev. Lett.*, **75** (1995) 4780.
[25] Rouyer F., Cohen-Addad S., Vignes-Adler M. and Höhler R., *Phys. Rev. E*, **67** (2003) 021405.
[26] Princen H. M. and Kiss A. D., *J. Colloid Interface Sci.*, **112** (1986) 427.
[27] Ono I. K. *et al.*, *Phys. Rev. Lett.*, **89** (2002) 095703.
[28] Lacasse M.-D. *et al.*, *Phys. Rev. Lett.*, **76** (1996) 3448.
[29] Bocquet L. *et al.*, *Phys. Rev. E*, **65** (2002) 011307.
[30] Liu A. *et al.*, *Phys. Rev. Lett.*, **76** (1996) 3017.